

# Precision measurement of the rotational energy-level structure of the three-electron molecule $\text{He}_2^+$

Luca Semeria,<sup>1</sup> Paul Jansen,<sup>1</sup> and Frédéric Merkt<sup>1,\*</sup>

<sup>1</sup>Laboratory of Physical Chemistry, ETH Zurich, CH-8093 Zurich, Switzerland

(Dated: November 4, 2021)

The term values of all rotational levels of the  $^4\text{He}_2^+ X^+ {}^2\Sigma_u^+$  ( $\nu^+ = 0$ ) ground vibronic state with rotational quantum number  $N^+ \leq 19$  have been determined with an accuracy of  $8 \times 10^{-4} \text{ cm}^{-1}$  ( $\sim 25 \text{ MHz}$ ) by MQDT-assisted Rydberg spectroscopy of metastable  $\text{He}_2^*$ . Comparison of these term values with term values recently calculated *ab initio* by Tung *et al.* [J. Chem. Phys. **136**, 104309 (2012)] reveal discrepancies that rapidly increase with increasing rotational quantum number and reach values of  $0.07 \text{ cm}^{-1}$  ( $\sim 2.1 \text{ GHz}$ ) at  $N^+ = 19$ .

PACS numbers: 34.50.Gb, 33.80.Rv, 34.80.Gs, 37.10.Mn

## I. INTRODUCTION

Predicting the energy level structure of molecules from first principles is one of the major goals and tasks of theoretical molecular physics and chemistry. Few-electron molecules such as  $\text{H}_2^+$ ,  $\text{H}_2$  and  $\text{He}_2^+$  are particularly attractive systems for comparison with experimental results because numerically “exact” predictions of molecular properties can in principle be obtained, i.e., predictions that are only limited in accuracy by the uncertainties of fundamental constants. For  $\text{H}_2^+$  and  $\text{H}_2$ , remarkable progress has been achieved by theoretical calculations in the past ten years [1–6]. The most precise theoretical calculations in these molecules are based on an effective nonrelativistic form of QED that treats relativistic and radiative effects perturbatively using the nonrelativistic wave functions. Remarkable progress has also been made in experimental determinations of energy intervals in these molecules [7–13] so that the prospect of exploiting the comparison of theoretical and experimental results in these systems to either improve the accuracy of fundamental constants [14] or uncover new physical phenomena [15, 16] becomes increasingly attractive. For instance, Salumbides *et al.* argue that precision measurements in molecules may reveal (or at least set upper bounds to potential effects of) so far unknown forces acting on nuclei at distances typical of molecular bonds [16, 17]. In general, precision measurements in simple systems are ideal to test theoretical predictions at the most fundamental level. The three-electron molecule  $\text{He}_2^+$ , with nuclei four times as heavy as those in  $\text{H}_2^{(+)}$ , is also an attractive molecular system in this context.

*Ab initio* calculations in  $\text{He}_2^+$  were carried out almost immediately after Heitler and London showed how to efficiently treat electron correlation in  $\text{H}_2$  [18]. Majorana [19] and Pauling [20] extended the Heitler-London method to predict the dissociation energy, the equilibrium distance, and the harmonic vibrational frequency of  $\text{He}_2^+$ . Since then, numerous calculations have been

reported on  $\text{He}_2^+$  (see, e.g., Refs. [21–32]). The most recent *ab initio* calculations of the energy-level structure of  $\text{He}_2^+$  by Tung *et al.* [32] provided almost exact nonrelativistic energies and an accuracy comparable to the accuracy of the best experimental results available on  $\text{He}_2^+$  in the literature, i.e., the 9 infrared rovibrational transition frequencies recorded between low-lying rovibrational levels in  $^3\text{He}^4\text{He}^+$  by Yu and Wing [33] and the 7 rovibronic transition frequencies measured between high-lying vibrational levels of the  $X^+ {}^2\Sigma_u^+$  electronic ground state of  $^4\text{He}_2^+$  and the weakly bound levels of the  $A^+ {}^2\Sigma_g^+$  state near the  $\text{He}^+ + \text{He}$  dissociation limit by Carrington and coworkers [34]. Tung *et al.* [32] reported the accuracy of their calculations to be limited by the neglect of relativistic and QED corrections, which they estimated to be on the order of  $0.004 \text{ cm}^{-1}$  (120 MHz) for the low-lying rovibrational levels of  $\text{He}_2^+$  by comparing such corrections in  $\text{H}_2$  with the relativistic correction calculated for the  $\nu = 0 - 1$  interval of  $^3\text{He}^4\text{He}^+$  [35].

Experimental measurements of the low-lying levels of  $^4\text{He}_2^+$  are complicated by the fact that  $^4\text{He}_2^+$  is apolar and has no electric-dipole-allowed vibrational and rotational transitions. Recently we have started systematic measurements of the energy-level structure of  $\text{H}_2^+$  and  $\text{He}_2^+$  by multichannel-quantum-defect-theory(MQDT)-assisted Rydberg spectroscopy of  $\text{H}_2$  [7, 9, 12, 36] and  $\text{He}_2$  [37, 38]. In the case of  $\text{He}_2^+$ , the procedure consists of measuring high-resolution spectra of triplet ( $S = 1$ ),  $np$  Rydberg states of very high principal quantum number  $n$  from the  $a {}^3\Sigma_u^+$  metastable state of  $\text{He}_2$  and extrapolating the Rydberg series to their limits using MQDT [39]. We report here the determination of the term values of all rotational levels of the  $X^+ {}^2\Sigma_u^+$  ( $\nu^+ = 0$ ) state of  $\text{He}_2^+$  up to the rotational level with rotational quantum number  $N^+ = 19$ , which is located more than  $2600 \text{ cm}^{-1}$  above the ground state of  $\text{He}_2^+$ . Surprisingly, we find that the deviations between measured and calculated term values rapidly increase with increasing  $N^+$  value.

\* merkt@xuv.phys.chem.ethz.ch

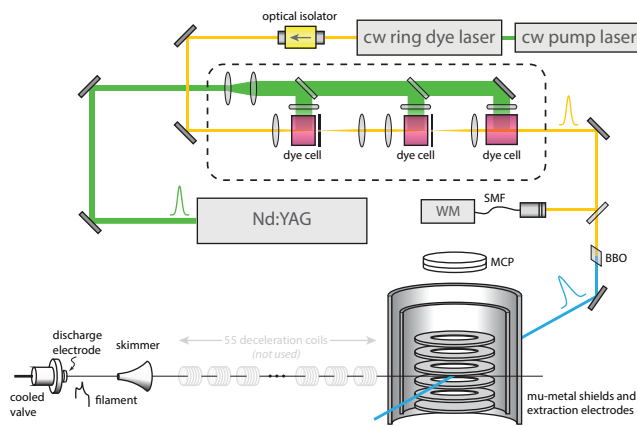


Figure 1. Schematic representation (not to scale) of the experimental setup. Shown are the pulsed-amplified ring-dye-laser system and spectrometer containing the discharge source, the Zeeman decelerator, and the magnetically shielded photoexcitation region. Nd:YAG, neodymium-doped yttrium aluminum garnet; WM, wavemeter; SMF, single-mode fiber; BBO, beta-barium-borate crystal; MCP, microchannel-plate detector.

## II. EXPERIMENTAL PROCEDURE

The experimental setup is presented schematically in Fig. 1 (see also Refs. [38] and [40]). The measurements were performed with a three-stage pulse-amplified laser system [41] that was seeded with the output of a continuous-wave (cw) ring dye laser and pumped by the second harmonic of a Q-switched neodymium-doped yttrium-aluminum-garnet (Nd:YAG) laser. The pulse-amplified output of the ring laser was frequency doubled in a beta-barium-borate crystal, resulting in near-Fourier-transform-limited pulses of UV radiation with a bandwidth of 180 MHz. The frequency was adjusted by scanning the seed-laser frequency.

Calibration of the laser fundamental frequency to an accuracy of 20 MHz ( $1\sigma$ ) was achieved by coupling a fraction of the pulse-amplified output of the ring laser into a wavemeter (HighFinesse WS7). To quantify the effects of the frequency chirp arising in the pulse-amplification process, part of the cw output of the ring laser was used to record the laser-induced-fluorescence spectrum of  $I_2$  so as to determine the difference between the frequencies of the cw and pulse-amplified outputs of the ring dye laser.

A supersonic beam of metastable helium molecules was produced in a source chamber by striking an electric discharge through an expansion of pure helium gas at the exit of a pulsed valve [42]. The body of the valve was cooled to a temperature of 77 K, resulting in a supersonic beam with a velocity of approximately 1000 m/s [43]. The molecular beam was collimated with a 2-mm-diameter skimmer before entering a second, differentially-pumped vacuum chamber containing a 55-stage Zeeman decelerator [43–45]. Although the Zeeman decelerator was not used to obtain the results presented below, it

played an important role in the initial assignment of the spectra and in the assessment of the systematic uncertainty resulting from the Doppler effect, as explained in Refs. [38] and [40].

After about 1 m of flight, the molecules entered a third vacuum chamber that was used for photoexcitation and detection. The photoexcitation region was surrounded by a cylindrically symmetric stack of electrodes for the application of ionization and extraction electric fields. The molecular beam crossed the UV laser beam at right angles on the symmetry axis of the electrode stack, which was oriented perpendicularly to the plane defined by the laser and molecular beams. High- $n$  Rydberg states were ionized by a pulsed electric field, which was also used to extract the ions toward a microchannel-plate (MCP) detector. The spectra were obtained by monitoring the pulse-field-ionization yield as a function of the UV laser wavenumber. The spectra were greatly simplified by applying a small electric field shortly after photoexcitation but before the field-ionization pulse. This first “discrimination” pulse did not only field ionize Rydberg states with  $n \gtrsim 200$ , but also shifted all ions produced by direct ionization or rapid autoionization (prompt ions) out of the photoexcitation volume. Consequently, the ions generated by the second, field-ionization pulse had different flight times to the MCP detector than the prompt ions and could be monitored separately. Stray electric fields were determined by recording spectra in the presence of different applied potentials across the stack and fitting the observed Stark shifts to a quadratic polynomial and were compensated to a level of better than 1 mV/cm, as explained in Ref. [46]. To suppress stray magnetic fields, two concentric mu-metal tubes were used to shield the photoexcitation region.

## III. RYDBERG SERIES OF $He_2$ AND MULTICHANNEL QUANTUM-DEFECT THEORY CALCULATIONS

With the exception of the single bound level of the electronic ground state, all bound states of  $He_2$  are Rydberg states [47]. The rotational levels of the  $a^3\Sigma_u^+$  metastable state and of high- $n$  Rydberg states are schematically depicted on the left-hand side of Fig. 2. The bosonic nature of the  $^4He$  nuclei excludes the existence of even rotational states in the  $a^3\Sigma_u^+$  ( $\nu'' = 0$ ) state of the neutral molecule and in the  $X^+{}^2\Sigma_u^+$  ( $\nu^+ = 0$ ) state of the ion, so that half of the energy levels is missing. In the following, we use double-primed symbols to indicate the quantum numbers of the metastable  $He_2$  molecule and symbols with a superscript “+” to indicate the quantum numbers of the molecular ion. Single-photon excitation from the metastable  $a^3\Sigma_u^+$  state, which is a triplet ( $S'' = 1$ ) Rydberg state of s character [48], primarily results in the excitation of p Rydberg series converging on the different rotational levels of the  $X^+{}^2\Sigma_u^+$  ground state of  $He_2^+$ . The spin-rotation splittings of the rotational levels of the  $X^+{}^2\Sigma_u^+$

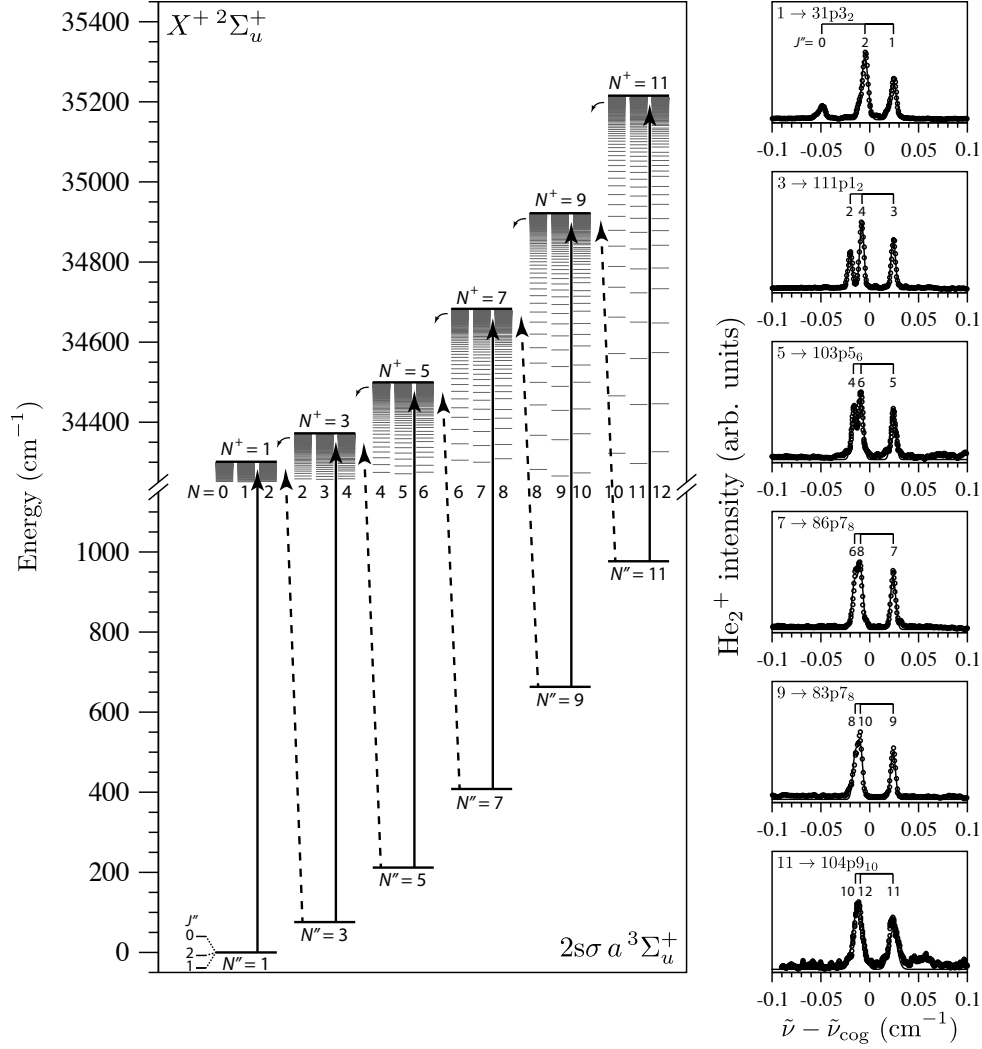


Figure 2. Left panel: energy-level diagram showing the lowest six rotational levels of  $\text{He}_2^+(a^3\Sigma_u^+, \nu'' = 0)$  and the triplet  $np$  Rydberg series of  $\text{He}_2$  converging on the lowest six rotational levels of  $\text{He}_2^+(X^+ 2\Sigma_u^+, \nu^+ = 0)$ . Full arrows represent the  $npN_N^+ \leftarrow N''$  series with  $N^+ = N''$  and  $N = N^+, N^+ + 1$  that were used to determine the ionization thresholds, while dashed arrows indicate  $npN_N^+ \leftarrow N''$  series with  $N^+ = N'' - 2$  and  $N = N^+ + 1$  that were used to determine the rotational structure of the  $a^3\Sigma_u^+ (\nu'' = 0)$  state of  $\text{He}_2$ . Curved arrows indicate the  $npN_N^+ \leftarrow N_{N^+ - 1}$  series that undergo rapid rotational autoionization above the  $N^+ - 2$  threshold. The fine structure of the initial state is not visible on the scale of the figure and is shown strongly magnified for the  $N'' = 1$  rotational state only. Right panels, top to bottom: Representative experimental spin-spin and spin-rotation fine structure observed for the lowest six rotational states of  $\text{He}_2^*$  (open circles) along with the fitted line profiles (full lines). The transitions are shown with respect to their fitted center of gravity (cog), with  $\tilde{\nu}_{\text{cog}} = 34\,258.516\,64, 34\,216.444\,42, 34\,277.233\,94, 34\,260.142\,15, 34\,003.792\,64$  and  $33\,934.843\,85\text{ cm}^{-1}$  from top to bottom.

ground state of  $\text{He}_2^+$  are not resolved in our spectra, so that the ionic rotational levels are adequately labeled by the rotational quantum number  $N^+$ . The total angular momentum (excluding spins)  $\vec{N}$  of the high Rydberg states results from the vector addition of  $\vec{N}^+$  with the Rydberg-electron orbital angular momentum  $\vec{\ell}$  so that  $N = N^+ + \ell, N^+ + \ell - 1, \dots, |N^+ - \ell|$ . For the p Rydberg states of interest here, this results in  $N = N^+, N^+ \pm 1$  (see Ref. [42] for details). Consequently, the Rydberg states can be labeled as  $npN_N^+$ . Each rotational level

of the  $a^3\Sigma_u^+$  metastable state is split into a triplet by the spin-spin and spin-rotation interactions [49]. The rotational levels are labeled by the rotational quantum number  $N''$  and the total angular momentum quantum number  $J''$  ( $J'' = N'', N'' \pm 1$ ). Each rotational level consists of a triplet with characteristic splittings, which are known extremely precisely from the high-resolution microwave studies of Lichten *et al.* [49, 50] and Bjerre *et al.* [51, 52]. Consequently, all transitions have a triplet structure with characteristic splittings and intensity patterns that can be used to assign the initial level in a

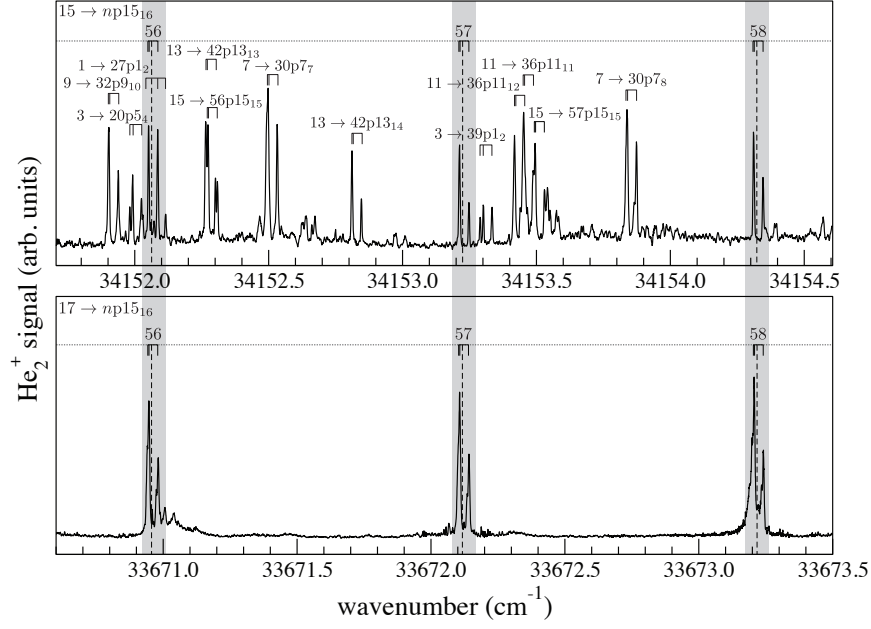


Figure 3. Determination of initial-state combination differences with the example of the  $np15_{16}$  Rydberg series recorded from the  $a^3\Sigma_u^+$ ,  $\nu'' = 0$ ,  $N'' = 15$  (upper panel) and  $N'' = 17$  (lower panel) in the region  $n = 56 - 58$ . The centers of gravity of the triplet structures are indicated by the vertical dashed lines. The background signal in the spectra is insignificant and the vertical scale is linear.

straightforward manner. Examples of these patterns for transitions originating from the  $N'' = 1 - 11$  levels are given on the right-hand side of Fig. 2. Three Gaussian functions of full width at half maximum of 180 MHz, separated by the known fine-structure intervals [49–53] and with relative intensities weighted by the  $2J'' + 1$  degeneracy factors, were used to convert each observed triplet into its “fine-structure-free” center of gravity. All transition wavenumbers reported in this article correspond to such centers of gravity.

Rydberg series converging on a particular  $(\nu^+, N^+)$  rovibrational level of the  $X^+2\Sigma_u^+$  electronic ground state of  $\text{He}_2^+$  are approximately described by Rydberg’s formula

$$\tilde{\nu}_{n\ell} = \tilde{\nu}_{N'', N^+} - \frac{\mathcal{R}_{\text{He}_2}}{(n - \delta_\ell)^2}, \quad \text{with } hc\tilde{\nu}_{N'', N^+} = E_1 + E_{\text{rv}}^+ - E_{\text{rv}}'', \quad (1)$$

where  $\tilde{\nu}_{n\ell}$  represents the spectral position of the Rydberg states of principal and orbital angular-momentum quantum numbers  $n$  and  $\ell$ , respectively, and quantum defect  $\delta_\ell$ . The quantities  $\mathcal{R}_{\text{He}_2}$  and  $E_1$  represent the mass-corrected Rydberg constant for  $\text{He}_2$  and the adiabatic ionization energy of metastable  $\text{He}_2$ , corresponding to the energy difference between the  $X^+2\Sigma_u^+$  ( $\nu^+ = 0$ ,  $N^+ = 1$ ) level of  $\text{He}_2^+$  and the  $a^3\Sigma_u^+$  ( $\nu'' = 0$ ,  $N'' = 1$ ) metastable level, respectively.  $E_{\text{rv}}^+$  and  $E_{\text{rv}}''$  are the rovibrational energies of the  $\text{He}_2^+$  ion core and of metastable  $\text{He}_2$  with respect to the  $(\nu^+ = 0, N^+ = 1)$  and  $(\nu'' = 0, N'' = 1)$  levels, respectively. Although Rydberg’s formula accu-

rately describes the essentially unperturbed  $npN_{N=N^+}^+$  series, it does not account for the interactions between series of the same  $N$  value that converge on different rotational states of  $\text{He}_2^+$ . For the  $np[N^+ = N + 1]_N$  series, these interactions give rise to spectral perturbations below, and to rotational autoionization above, the  $N^+ = N - 1$  thresholds (see Fig. 2) and can be accounted for in the framework of multichannel quantum-defect theory [39, and references therein].

In this work, we determined the ionization thresholds corresponding to the different rotational levels of  $\text{He}_2^+$  with respect to the  $N'' = 1$  rotational state of  $\text{He}_2^*$  by extrapolating Rydberg series of metastable helium molecules using the MQDT program developed by Jungen [39]. The data used for the extrapolation consist of  $np$  Rydberg series with  $n$  ranging from 95 to 110, excited from the  $\nu'' = 0$  and  $N'' \leq 19$  levels of metastable  $\text{He}_2$ .

The quantum-defect parameters for the *gerade* triplet  $np$  and  $nf$  Rydberg states of  $\text{He}_2$ , derived by Sprecher *et al.* [37], was adopted without change for the extrapolation of the Rydberg series. In Ref. [37], internuclear-distance( $R$ )-dependent and energy( $\epsilon$ )-dependent  $\eta$  eigenquantum-defect matrices were extracted from data available in the literature on  $np$  and  $nf$  Rydberg levels with  $n$  in the range 2–39,  $v^+ \leq 2$ , and  $N^+ \leq 19$  in a least-squares-fit procedure. High- $n$  Rydberg states were not used in the fit, because the level energies of high- $n$  Rydberg states are insensitive to adjustments of the quantum defects, a fact that is also exploited in the present analysis (see Ref. [37] for

details).

#### IV. DATA ANALYSIS AND RESULTS

The dominant  $npN^+ \leftarrow a^3\Sigma_u^+(\nu'' = 0, N'')$  Rydberg series in the spectrum of  $\text{He}_2$  are those with  $N^+ = N''$ . There are three such series with  $N = N^+, N^+ \pm 1$ . However, all  $npN_{N+1}^+$  Rydberg states with  $N^+ > 1$  located above the  $N^+ - 2$  ionization thresholds are subject to rapid autoionization, because of the strong coupling, indicated by the curved arrows in Fig. 2, between channels of the same value of  $N$ , but differing in  $N^+$  by 2 [37, 42]. The corresponding transitions are strongly broadened and thus not detectable in our high-resolution spectra. Below the  $N^+ - 2$  ionization thresholds, the autoionization of the  $npN_{N+1}^+$  Rydberg states is suppressed but the coupling between the  $npN_{N+1}^+$  and  $np[N^+ - 2]_{N+1}$  channels leads to strong perturbations and mixing of the Rydberg series. The  $npN_{N+1}^+$  series is always observable from both the  $N'' = N^+$  (full arrows in Fig. 2) and  $N'' = N^+ - 2$  (dashed arrows in Fig. 2) rotational levels of the metastable state, which enables one to determine the relative position of the  $N'' - 2$  and  $N''$  levels by building combination differences.

To obtain a full set of rotational intervals in the  $a^3\Sigma_u^+$  state of  $\text{He}_2$  and the  $X^+2\Sigma_u^+$  state of  $\text{He}_2^+$ , we proceeded in two steps. First, initial-state combination differences  $\tilde{\nu}_{N''-2, N''}$ , i.e., the energy intervals between the  $N'' - 2$  and  $N''$  rotational levels, were determined as illustrated in Fig. 3 with the example of the  $N'' = 15$  and 17 levels, where the upper and lower panels show the  $np15_{16}$  series around  $n = 57$  recorded from the  $N'' = 15$  and  $N'' = 17$  levels, respectively. Each member of this series observed from both rotational levels represents an independent measurement of  $\tilde{\nu}_{15,17}$ . The differences between the centers of gravity of the triplets (marked by vertical dashed lines) give a value of  $481.1061(7) \text{ cm}^{-1}$  for the interval between the  $a^3\Sigma_u^+$ ,  $\nu'' = 0, N'' = 15$  and 17 levels. All transitions used to determine the rotational structure of the  $a^3\Sigma_u^+$  state are listed in Table S1 of the Supplementary Material. These transitions form a redundant network, from which the relative positions of all states connected by the transitions can be determined in a global fit, as described in Ref. [54]. The rotational term values of the  $a^3\Sigma_u^+$  ( $\nu'' = 0$ ) metastable state of  $\text{He}_2$  presented in the third column of Table I could be determined in this way up to  $N'' = 19$ . These term values agree, within the respective uncertainties, with the rotational term values we calculated with the rotational constants reported by Focsa *et al.* [53] and presented in the second column of Table I.

In the second step, the positions of the rotational levels of the  $\text{He}_2^+$  ion were determined by extrapolating  $np[N^+ = N'']_{N^+, N^+ \pm 1} \leftarrow N''$  series. Figure 4 presents spectra of the  $np[N^+ = N'']_{N^+, N^+ \pm 1} \leftarrow N''$  Rydberg series recorded for this purpose, and Table II lists

the corresponding transition wavenumbers. The choice of the range of principal quantum number between 95 and 110 used for the extrapolation represented the best compromise between maximal accuracy of the Rydberg-series extrapolation, which is reached at the highest possible values of  $n$ , and minimal systematic uncertainties in the wavenumber measurements. In our experiments (see discussion below), the dominant source of systematic uncertainty comes from Stark-shifts induced by residual electric fields, which could be compensated to  $1 \text{ mV/cm}$ . This uncertainty amounts to  $10 \text{ MHz}$  at  $n = 110$  and scales with  $n^7$ , which made extrapolations based on transitions including Rydberg states with  $n > 110$  insufficiently accurate.

The spectra depicted in Fig. 4 all reveal at least one of the two expected series. In some spectra, such as the spectrum of the  $np1_{1,2} \leftarrow 1$  transitions, perturbations lead to regions where the two series are clearly distinguishable (e.g., in the region  $n = 100 - 105$  and above  $n = 109$  in the  $np1_{1,2}$  series). In other spectra, the two series are difficult to distinguish because of the partially overlapping fine structure and reliable “fine-structure-free” positions can only be derived from the analysis of lineshapes.

In an initial fit, the  $np19_{20} \leftarrow 19$  series was excluded, because of its interaction with the  $np21_{20}$  series which could not be measured at sufficiently high  $n$  values for the  $N^+ = 21$  threshold to be accurately determined. The rotational energy levels with  $N^+ \leq 19$  obtained in this way were used to derive a set of effective rotational constants that was subsequently used to predict the term value of the  $N^+ = 21$  level with respect to the  $N^+ = 1$  level ( $3158.115 \text{ cm}^{-1}$ ). The ionization thresholds of all series, including the  $np19_{20}$  series, were then determined in a second fit for which the  $N^+ = 21$  threshold was fixed at the predicted value. The relative positions of the ionic rotational states obtained from the transition wavenumbers listed in Table II and from the known positions of the rotational levels of the metastable state (see third column of Table I) are listed in the last column of Table I, where they are compared with the results of the *ab initio* calculations of Tung *et al.* [32]. The adiabatic ionization energy of  $\text{He}_2$  ( $a^3\Sigma_u^+$ ), defined as the interval between the  $a^3\Sigma_u^+$  ( $\nu'' = 0, N'' = 1$ ) state of  $\text{He}_2$  and the  $X^+2\Sigma_u^+$  ( $\nu^+ = 0, N^+ = 1$ ) state of  $\text{He}_2^+$ , is found to be  $34\,301.205\,65(12) \pm 0.0014_{\text{sys}} \text{ cm}^{-1}$ , as already reported in Ref. [38].

Table III summarizes the main sources of systematic and statistical uncertainty in the determination of ionization thresholds and  $\text{He}_2^+$  rotational intervals. The main source of statistical uncertainty comes from the lineshape analysis and the wavenumber calibration ( $25 \text{ MHz}$ ), resulting from the accuracy of the wavemeter. The systematic uncertainty of the ionization thresholds is larger ( $40 \text{ MHz}$ ) than that of the rotational intervals because the absolute calibration error cancels out when building combination differences. Although the absolute accuracy of the wave-meter measurements is specified as  $20 \text{ MHz}$ , the



Table I. Rotational term values of the  $a^3\Sigma_u^+(\nu'' = 0)$  state of  $\text{He}_2$  (3rd column) and the  $X^+{}^2\Sigma_u^+(\nu^+ = 0)$  ground state of  $\text{He}_2^+$  (6th column). For comparison, term values calculated with the molecular constants for the  $a^3\Sigma_u^+(\nu'' = 0)$  state of  $\text{He}_2$  reported by Focsa *et al.* [53] and the term values of the  $X^+{}^2\Sigma_u^+(\nu^+ = 0)$  state of  ${}^4\text{He}_2^+$  calculated *ab initio* by Tung *et al.* [32], are shown in the 2nd and 5th columns respectively. All values are given in  $\text{cm}^{-1}$ .

$N''$	Ref. [53] <sup>a</sup> (FTIR)	This work	$N^+$	Ref. [32] ( <i>ab initio</i> )	This work <sup>b</sup> (MQDT fit)
1	0	0	1	0	0
3	75.8129(3)	75.8136(8)	3	70.936	70.9379(8)
5	211.9937(8)	211.9950(8)	5	198.359	198.3647(8)
7	408.0605(16)	408.0614(8)	7	381.822	381.8346(8)
9	663.322(3)	663.3231(8)	9	620.683	620.7021(9)
11	976.879(4)	976.8809(8)	11	914.112	914.1367(8)
13	1347.638(7)	1347.6396(8)	13	1261.089	1261.1242(8)
15	1774.307(11)	1774.3072(8)	15	1660.420	1660.4627(9)
17	2255.413(17)	2255.4133(8)	17	2110.736	2110.7932(9)
19	2789.31(3)	2789.3056(8)	19	2610.505	2610.5744(9)

<sup>a</sup> Calculated using the rotational constants reported by Focsa *et al.* [53].

<sup>b</sup> The observed rotational term values can be described by  $B_0^+ = 7.101\,143(25)\,\text{cm}^{-1}$ ,  $D_0^+ = 5.2156(36) \times 10^{-4}\,\text{cm}^{-1}$ ,  $H_0^+ = 3.29(16) \times 10^{-8}\,\text{cm}^{-1}$ , and  $L_0^+ = -7.3(22) \times 10^{-12}\,\text{cm}^{-1}$ .

intrinsic Allan deviation over periods shorter than 1 min lies typically around 300 kHz [55, 56]. Long-term fluctuations of the wavemeter were monitored by recording a small part of the spectrum prior to each measurement and performing a statistical analysis of the fitted line positions. The resulting histogram is shown in Fig. 5 and resembles a Gaussian distribution with a standard deviation of 25(5) MHz in the UV. This uncertainty of 25 MHz approximately corresponds to the specified relative accuracy of the wavemeter of 10 MHz in the fundamental and contributes a statistical uncertainty of 25 MHz to the rotational intervals. The uncertainty of the Rydberg-series extrapolation by MQDT is dominated by the uncertainty in the quantum-defect parameters reported in Ref. [37] and is only 3 MHz for the ionization energy and 6 MHz for the rotational intervals. This uncertainty does not cancel out when determining the relative positions of the ionic levels because the series of different  $N$  values were extrapolated separately.

The remaining systematic uncertainties are dominated by the contribution of the Stark shift resulting from the residual electric field. The other sources of systematic uncertainties only affect the value of the ionization energy because they cancel out when determining the relative positions of the ionic rotational levels.

As explained in Sec. II, the stray electric field was determined and subsequently compensated by recording Rydberg spectra in the presence of different dc electric-field strengths and fitting the observed Stark shifts to a quadratic polynomial. Stray magnetic fields were suppressed by surrounding the photoexcitation region by two concentric mu-metal shields. The contribution of Stark and Zeeman shifts induced by residual electric and magnetic fields are 10 and 1 MHz, respectively. No shift in the line positions was observed when the laser power and the nozzle-stagnation pressure were varied, and the contri-

butions of ac-Stark and pressure shifts to the systematic uncertainties is estimated to be at most 2 and 1 MHz, respectively. Uncertainties from Doppler shifts were determined to be around 5 MHz.

## V. DISCUSSION AND CONCLUSIONS

The most precise *ab initio* calculations of the rovibrational energy levels of  $\text{He}_2^+$  reported so far have been carried out by Tung *et al.* [32]. The calculations relied on the use of 1200 explicitly correlated Gaussian functions with shifted centers in the range of internuclear distances between  $R = 0.9$  and  $100\,a_0$  to obtain the Born-Oppenheimer potential energy function. To derive accurate rovibrational energies, Tung *et al.* [32] also calculated the adiabatic corrections and included nonadiabatic corrections by using  $R$ -independent effective reduced masses in the vibrational and rotational kinetic operators in the Hamiltonian. Relativistic and radiative corrections were neglected, but using an argument based on scaling these corrections from the values they take in  $\text{H}_2$  [5] to the relativistic correction for the first vibrational interval of  ${}^3\text{He}{}^4\text{He}^+$  [35] and assuming that these corrections are mass independent, they estimated their predictions of the lowest vibrational interval in  $\text{He}_2^+$  to have an accuracy of about  $0.004\,\text{cm}^{-1}$ , or 120 MHz.

Comparison of our experimental results with the predictions of Tung *et al.* [32], we find that the experimental term values always lie above the calculated ones, and that the discrepancies rapidly increase with increasing rotational quantum number (see Fig. 6), reaching a value of almost  $0.07\,\text{cm}^{-1}$  (2.1 GHz) at  $N^+ = 19$ , which is more than ten times larger than the estimated uncertainty of the calculations. In reconstructing the argument of Tung *et al.* [32], we found that the rela-

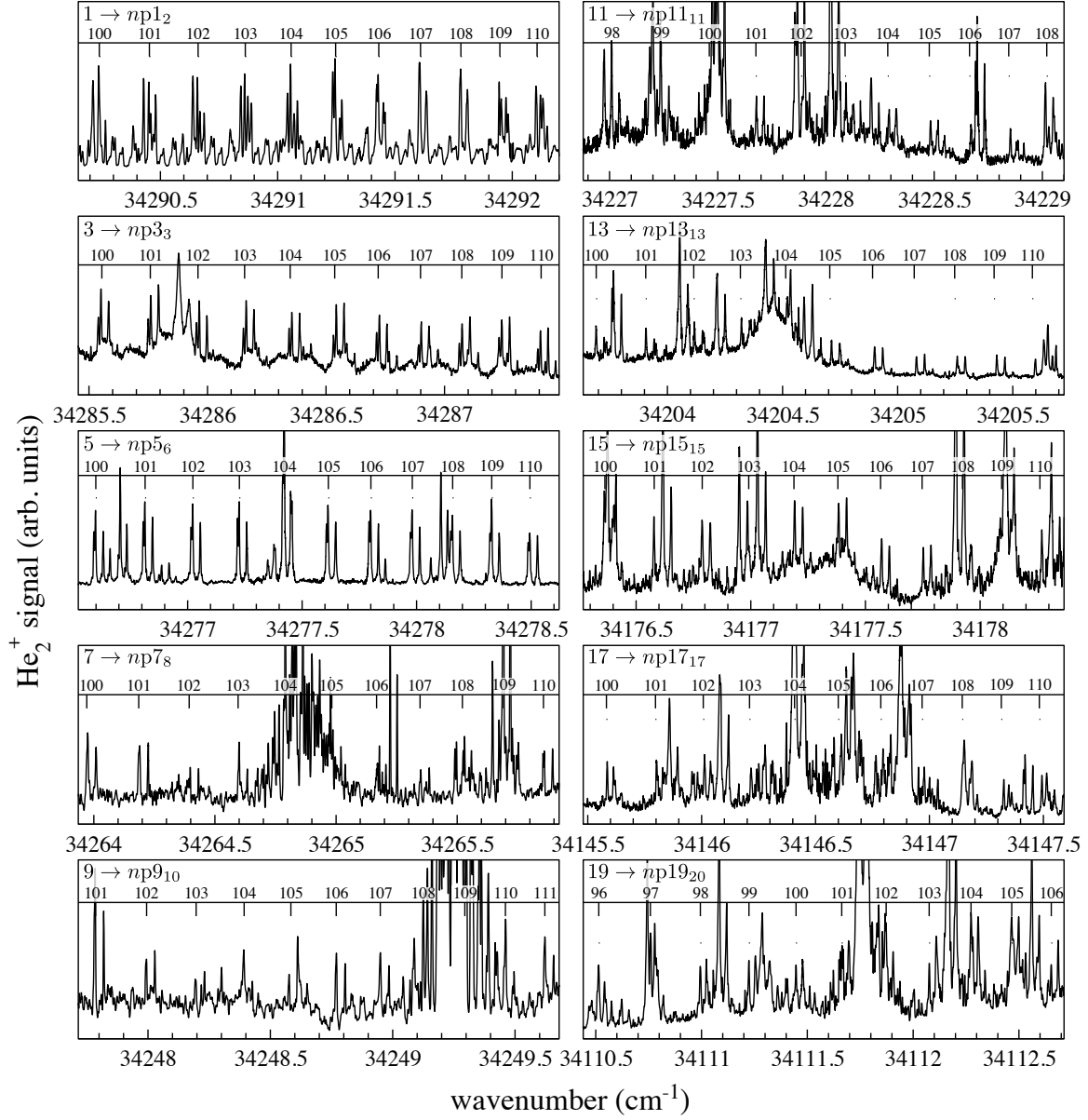


Figure 4. Spectra of the  $npN_N^+ \leftarrow a^3\Sigma_u^+ (\nu'' = 0, N'')$  series of  $\text{He}_2$  with  $N^+ = N'' \leq 19$ ,  $N = N^+, N^+ + 1$  and  $n$  around 100. For clarity, assignment bars are only shown for a single series in each spectrum. The background signal in the spectra is insignificant and the vertical scale is linear.

tivistic ( $-0.0026 \text{ cm}^{-1}$ ) and radiative ( $0.0010 \text{ cm}^{-1}$ ) corrections of the first rotational interval of  $\text{H}_2$  [5], rather than the first vibrational interval, were used to scale the relativistic correction of the first vibrational interval in  $^3\text{He}^4\text{He}^+$  ( $-0.006 \text{ cm}^{-1}$ ) [35]. When we scaled the relativistic ( $-0.0234 \text{ cm}^{-1}$ ) and radiative ( $0.0213 \text{ cm}^{-1}$ ) corrections of the  $(\nu, J) : (0, 0) \rightarrow (1, 0)$  interval in  $\text{H}_2$  [5], we found a correction of  $0.0005 \text{ cm}^{-1}$ , or 15 MHz, for this interval in  $^3\text{He}^4\text{He}^+$ . Following the argument of Tung *et al.*, we scaled the relativistic and radiative corrections of the rotational states of  $\text{H}_2$  [5] by the factor 3.9. The results are displayed as the dashed line in Fig. 6. The

scaled corrections appear to account for the discrepancies between experimental and calculated rotational term values reasonably well up to  $N^+ = 11$ , but rapidly become inadequate beyond  $N^+ = 11$ . Further work is required to understand the origin of this discrepancy. It is conceivable that the approximate treatment of the nonadiabatic correction through  $R$ -independent reduced masses in Ref. [32] becomes increasingly inaccurate as  $N^+$  increases.

The results presented in this article suggest that even the best *ab initio* calculations available in the literature on the three-electron molecule  $\text{He}_2^+$  are still far from

Table II. Observed transitions from the  $a^3\Sigma_u^+$  ( $\nu'' = 0, N''$ ) state of  $^4\text{He}_2$  to the  $npN_N^+$  Rydberg states belonging to series converging to the  $X^+{}^2\Sigma_u^+$  ( $\nu^+ = 0, N^+$ ) states of  $^4\text{He}_2^+$  and comparison with the results of MQDT calculations. The symbol  $\Delta$  represents the difference between observed and calculated line positions ( $\Delta = \text{obs.} - \text{calc.}$ ). All values are given in  $\text{cm}^{-1}$ . Missing entries correspond to transitions that were not observed or to strongly blended transitions.

$n$	$1 \rightarrow np1_1$		$1 \rightarrow np1_2$		$3 \rightarrow np3_3$		$3 \rightarrow np3_4$	
	$\tilde{\nu}_{\text{obs}}$	$\Delta$	$\tilde{\nu}_{\text{obs}}$	$\Delta$	$\tilde{\nu}_{\text{obs}}$	$\Delta$	$\tilde{\nu}_{\text{obs}}$	$\Delta$
97	34 289.526 24	-0.000 04	34 289.562 34	0.000 33	34 284.650 92	-0.000 25	34 284.580 58	-0.000 19
98	34 289.763 34	-0.000 25	34 289.794 96	0.000 12	34 284.888 50	0.000 02	34 284.799 30	-0.000 11
99	34 289.993 61	-0.000 13	34 290.021 53	0.000 34	34 285.118 83	0.000 20	34 285.012 32	-0.000 22
100	34 290.217 09	0.000 08	34 290.241 41	0.000 32	34 285.341 80	-0.000 10		
101	34 290.433 68	0.000 00	34 290.455 30	0.000 63	34 285.558 61	0.000 04		
102	34 290.644 09	0.000 08	34 290.662 49	0.000 41	34 285.769 19	0.000 29		
103	34 290.848 40	0.000 17	34 290.863 74	0.000 29	34 285.973 26	0.000 14	34 286.031 32	-0.000 45
104	34 291.046 69	0.000 10	34 291.059 38	0.000 25	34 286.171 32	-0.000 16	34 286.224 84	0.000 63
105	34 291.239 61	0.000 31	34 291.249 28	0.000 93	34 286.364 07	-0.000 12	34 286.412 41	0.000 32
106	34 291.426 71	0.000 13	34 291.433 64	0.001 36	34 286.551 46	-0.000 01	34 286.595 61	0.000 27
107					34 286.733 20	-0.000 33	34 286.774 26	0.000 29
108					34 286.909 93	-0.000 61	34 286.948 13	0.000 10
109	34 291.958 07	-0.000 01	34 291.949 02	0.000 23	34 287.082 15	-0.000 55	34 287.117 89	0.000 27
110	34 292.124 79	-0.000 55	34 292.107 16	-0.000 53	34 287.249 73	-0.000 46	34 287.283 64	0.000 80
111	34 292.287 99	-0.000 31	34 292.257 90	-0.000 48	34 287.412 91	-0.000 25	34 287.444 33	0.000 54
112	34 292.446 64	-0.000 28	34 292.399 93	-0.000 38				
$n$	$5 \rightarrow np5_5$		$5 \rightarrow np5_6$		$7 \rightarrow np7_7$		$7 \rightarrow np7_8$	
	$\tilde{\nu}_{\text{obs}}$	$\Delta$	$\tilde{\nu}_{\text{obs}}$	$\Delta$	$\tilde{\nu}_{\text{obs}}$	$\Delta$	$\tilde{\nu}_{\text{obs}}$	$\Delta$
95	34 275.399 57	0.000 04	34 275.427 33	0.000 11	34 262.802 52	0.000 09	34 262.806 98	-0.000 10
96	34 275.651 56	-0.000 52	34 275.678 34	0.000 45				
97	34 275.896 92	0.000 07	34 275.921 23	0.000 36	34 263.299 79	0.000 05		
98	34 276.134 04	-0.000 12	34 276.156 71	0.000 22				
99	34 276.363 93	-0.000 37	34 276.385 36	0.000 33				
100	34 276.587 38	-0.000 20	34 276.607 01	0.000 25				
101	34 276.803 83	-0.000 42	34 276.822 30	0.000 34				
102	34 277.014 20	-0.000 37	34 277.031 16	0.000 27	34 264.417 82	0.000 39	34 264.407 66	0.000 47
103	34 277.217 90	-0.000 90	34 277.233 94	0.000 14	34 264.621 58	-0.000 04	34 264.609 38	0.000 16
104			34 277.431 31	0.000 09	34 264.819 30	-0.000 30	34 264.805 33	-0.000 02
105			34 277.622 36	0.000 24				
106			34 277.808 48	0.000 29	34 265.200 41	0.000 32	34 265.180 98	0.000 19
107	34 277.978 14	-0.001 06	34 277.989 26	0.000 21	34 265.381 88	-0.000 24	34 265.360 24	-0.000 25
108	34 278.155 11	-0.001 10	34 278.165 09	0.000 20	34 265.558 76	-0.000 37	34 265.534 86	-0.000 25
109			34 278.336 71	0.000 80	34 265.731 58	0.000 29	34 265.704 51	-0.000 34
110			34 278.503 42	0.001 14			34 265.869 85	-0.000 03
$n$	$9 \rightarrow np9_9$		$9 \rightarrow np9_{10}$		$11 \rightarrow np11_{11}$		$11 \rightarrow np11_{12}$	
	$\tilde{\nu}_{\text{obs}}$	$\Delta$	$\tilde{\nu}_{\text{obs}}$	$\Delta$	$\tilde{\nu}_{\text{obs}}$	$\Delta$	$\tilde{\nu}_{\text{obs}}$	$\Delta$
95					34 226.284 84	-0.000 40	34 226.327 83	0.000 28
96					34 226.537 70	-0.000 07	34 226.578 89	0.000 52
97					34 226.782 51	-0.000 03	34 226.821 74	0.000 23
98					34 227.019 52	-0.000 32	34 227.057 85	0.000 57
99					34 227.250 19	0.000 21	34 227.285 85	-0.000 12
100								
101	34 247.811 32	-0.000 84	34 247.794 65	-0.000 56	34 227.690 02	0.000 10	34 227.723 74	0.000 52
102	34 248.023 25	-0.000 11	34 248.003 94	-0.000 50	34 227.900 13	-0.000 11	34 227.932 72	0.000 42
103	34 248.227 07	-0.000 44	34 248.207 04	0.000 86	34 228.103 35	-0.001 11	34 228.135 95	0.000 61
104			34 248.402 10	-0.000 01	34 228.301 68	-0.001 13	34 228.333 51	0.000 94
105			34 248.587 08	-0.003 17	34 228.495 11	-0.000 41	34 228.524 68	0.000 47
106	34 248.806 35	0.000 53	34 248.780 80	-0.000 30	34 228.682 71	-0.000 09		
107	34 248.987 51	-0.000 35	34 248.960 20	-0.000 14	34 228.864 15	-0.000 69	34 228.891 15	-0.000 41
108			34 249.136 06	0.001 18	34 229.041 69	-0.000 16		
109			34 249.304 31	-0.000 73				
110	34 249.505 50	0.000 99	34 249.470 92	0.000 30			34 229.405 79	0.000 23

continued on next page

reaching the same level of agreement with experimental data as in the two-electron molecule  $\text{H}_2$  [4, 5, 9–11].

## SUPPLEMENTARY MATERIAL

See Supplementary Material at [address to be inserted by Editor] for the wavenumbers of all transitions used to derive the rotational level energies of the  $a^3\Sigma_u^+$  ( $\nu'' = 0$ ) state of  $\text{He}_2$ .

## ACKNOWLEDGMENTS

We thank Christian Jungen (Laboratoire Aimé Cotton du CNRS, Orsay) for allowing us to use his MQDT program and Hansjürg Schmutz and Josef Agner for their expert technical assistance. This work is supported financially by the Swiss National Science Foundation under Project Nos. 200020-159848 and 200020-149216 and the NCCR QSIT. P.J. gratefully acknowledges ETH Zurich for support through an ETH fellowship.



Table II. –*Continued*

$n$	$13 \rightarrow np13_{13}$		$13 \rightarrow np13_{14}$		$15 \rightarrow np15_{15}$		$15 \rightarrow np15_{16}$	
	$\tilde{\nu}_{\text{obs}}$	$\Delta$	$\tilde{\nu}_{\text{obs}}$	$\Delta$	$\tilde{\nu}_{\text{obs}}$	$\Delta$	$\tilde{\nu}_{\text{obs}}$	$\Delta$
95					34 175.184 30	–0.000 85	34 175.232 64	–0.000 70
96	34 202.766 38	–0.000 54	34 202.819 75	–0.000 30	34 175.437 46	–0.000 22		
97	34 203.011 09	–0.000 58	34 203.062 27	–0.000 39	34 175.681 58	–0.000 85	34 175.728 09	0.001 02
98	34 203.248 13	–0.000 83	34 203.297 39	–0.000 55	34 175.919 62	–0.000 11	34 175.963 13	0.000 41
99	34 203.478 55	–0.000 54	34 203.526 25	0.000 08	34 176.149 54	–0.000 33	34 176.192 44	0.001 14
100	34 203.701 53	–0.000 82	34 203.747 80	0.000 17			34 176.412 76	–0.000 32
101	34 203.918 40	–0.000 61	34 203.962 97	0.000 38	34 176.590 00	0.000 21	34 176.628 50	0.000 17
102	34 204.129 53	0.000 21	34 204.172 03	0.000 74	34 176.799 39	–0.000 71		
103	34 204.333 55	0.000 02						
104	34 204.533 44	0.001 56	34 204.571 22	0.000 34	34 177.202 82	0.000 16		
105	34 204.724 62	0.000 04	34 204.764 64	0.002 43	34 177.394 19	–0.001 18	34 177.429 73	0.000 82
106	34 204.911 72	–0.000 13	34 204.948 54	0.000 37	34 177.581 25	–0.001 39	34 177.614 78	–0.000 30
107	34 205.093 57	–0.000 33	34 205.129 12	0.000 15	34 177.763 08	–0.001 60	34 177.796 00	–0.000 06
108	34 205.270 96	0.000 06						
109	34 205.442 72	–0.000 34	34 205.476 35	0.000 53				
110	34 205.610 31	–0.000 22			34 178.280 90	–0.000 42		
<hr/>								
$n$	$17 \rightarrow np17_{17}$		$17 \rightarrow np17_{18}$		$19 \rightarrow np19_{19}$		$19 \rightarrow np19_{20}$	
	$\tilde{\nu}_{\text{obs}}$	$\Delta$	$\tilde{\nu}_{\text{obs}}$	$\Delta$	$\tilde{\nu}_{\text{obs}}$	$\Delta$	$\tilde{\nu}_{\text{obs}}$	$\Delta$
95	34 144.410 06	0.000 41	34 144.442 31	0.000 18			34 110.275 32	0.001 58
96	34 144.661 17	–0.001 01	34 144.694 19	0.000 75	34 110.551 35	–0.000 08	34 110.524 19	–0.001 12
97	34 144.906 04	–0.000 89	34 144.937 09	0.000 07	34 110.796 83	0.000 68		
98	34 145.143 92	–0.000 31	34 145.173 17	–0.000 03	34 111.033 32	–0.000 11	34 111.006 06	0.000 39
99	34 145.372 91	–0.001 45	34 145.402 04	–0.000 24	34 111.264 53	0.000 98	34 111.234 89	–0.000 17
100	34 145.597 43	–0.000 19	34 145.624 02	–0.000 51	34 111.488 17	0.001 37	34 111.457 59	–0.000 03
101	34 145.814 64	0.000 36			34 111.702 24	–0.001 21		
102	34 146.024 88	0.000 29	34 146.049 52	–0.000 11				
103	34 146.228 90	0.000 10	34 146.254 15	0.001 18			34 112.086 48	–0.000 52
104					34 112.317 75	0.001 45		
105					34 112.508 60	–0.000 40		
106	34 146.807 23	0.000 12			34 112.696 34	0.000 08	34 112.663 06	–0.000 88
107	34 146.988 07	–0.001 08			34 112.879 55	0.001 25	34 112.845 05	–0.000 55
108	34 147.166 22	0.000 06	34 147.186 99	0.000 48	34 113.054 43	–0.000 87	34 113.022 26	–0.000 01
109	34 147.337 84	–0.000 47	34 147.359 28	0.001 28	34 113.227 23	–0.000 22	34 113.193 94	–0.000 18
110	34 147.504 69	–0.001 09	34 147.526 05	0.001 21	34 113.394 80	–0.000 12		

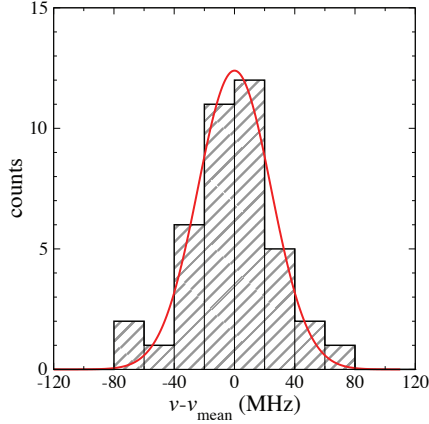


Figure 5. Histogram to quantify the relative accuracy of the wavemeter using the distribution of transition wavenumbers of the  $124p1_2 \leftarrow 1$  transition determined in independent calibration spectra recorded before each measurement. The solid line represents a Gaussian fit to the data with a standard deviation of 25 MHz.

- 
- [1] V. I. Korobov, *Phys. Rev. A* **74**, 052506 (2006).
  - [2] V. I. Korobov, *Phys. Rev. A* **77**, 022509 (2008).
  - [3] V. I. Korobov, L. Hilico, and J.-P. Karr, *Phys. Rev. Lett.* **112**, 103003 (2014).
  - [4] K. Piszczatowski, G. Łach, M. Przybytek, J. Komasa, K. Pachucki, and B. Jeziorski, *J. Chem. Theory Comput.* **5**, 3039 (2009).
  - [5] J. Komasa, K. Piszczatowski, G. Łach, M. Przybytek, B. Jeziorski, and K. Pachucki, *J. Chem. Theory Comput.*

Table III. Estimated statistical ( $1\sigma$ ) and systematic contributions to the uncertainty in the determinations of the ionization threshold of the  $a^3\Sigma_u^+$  state of  $\text{He}_2^+$  (second column) and rotational intervals of the  $\text{He}_2^+ X^+ {}^2\Sigma_u^+$ ,  $\nu^+ = 0$  ground state (third column). All values are given in MHz.

Source	$E_I$	$\tilde{\nu}_{N^++2,N^+}$
<i>Statistical</i>		
Wavenumber calibration	0	25
Determination of line centers	2	3
MQDT fit	3	5-8
Total statistical	4	26
<i>Systematic</i>		
Wavenumber calibration	40	0
AC-Stark shift	2	0
DC-Stark shift	10	5
Zeeman shift	1	0
Doppler shift	5	0
Pressure shift	1	0
Total systematic	42	5

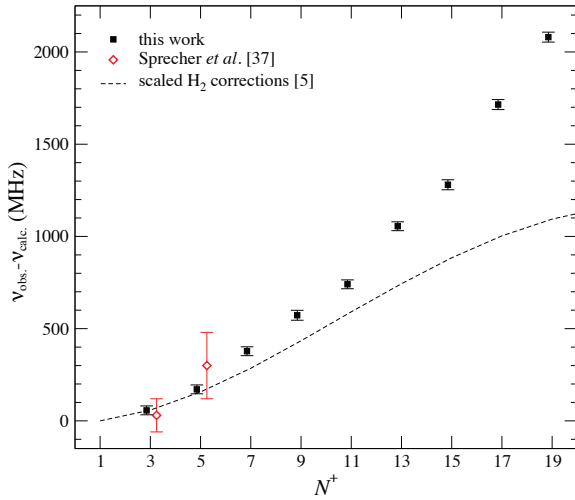


Figure 6. Differences between experimental (this work) and theoretical rotational term values (from Ref. [32]) in the  $X^+ {}^2\Sigma_u^+$  ( $\nu^+ = 0$ ) state of  $\text{He}_2^+$  (full squares). The experimental results of Sprecher *et al.* [37] are plotted as diamonds. The dashed line represents the corrections to the energy levels of molecular hydrogen that were scaled to the relativistic correction of the fundamental vibration in  ${}^3\text{He}{}^4\text{He}^+$  (see text).

7, 3105 (2011).

[6] M. Puchalski, J. Komasa, P. Czachorowski, and K. Pachucki, arXiv:1608.07081 [hep-ph, physics:physics] (2016), arXiv:1608.07081 [hep-ph, physics:physics].

[7] A. Osterwalder, A. Wüest, F. Merkt, and C. Jungen, *J. Chem. Phys.* **121**, 11810 (2004).

[8] J. C. J. Koelemeij, B. Roth, A. Wicht, I. Ernsting, and S. Schiller, *Phys. Rev. Lett.* **98**, 173002 (2007).

[9] J. Liu, E. J. Salumbides, U. Hollenstein, J. C. J. Koelemeij, K. S. E. Eikema, W. Ubachs, and F. Merkt, *J. Chem. Phys.* **130**, 174306 (2009).

[10] E. J. Salumbides, G. D. Dickenson, T. I. Ivanov, and W. Ubachs, *Phys. Rev. Lett.* **107**, 043005 (2011).

[11] G. D. Dickenson, M. L. Niu, E. J. Salumbides, J. Komasa, K. S. E. Eikema, K. Pachucki, and W. Ubachs, *Phys. Rev. Lett.* **110**, 193601 (2013).

[12] C. Haase, M. Beyer, C. Jungen, and F. Merkt, *J. Chem. Phys.* **142**, 064310 (2015).

[13] J. Biesheuvel, J.-P. Karr, L. Hilico, K. S. E. Eikema, W. Ubachs, and J. C. J. Koelemeij, *Nat. Commun.* **7**, 10385 (2016).

[14] W. H. Wing, G. A. Ruff, W. E. Lamb, and J. J. Spezeski, *Phys. Rev. Lett.* **36**, 1488 (1976).

[15] S. Schiller and V. Korobov, *Phys. Rev. A* **71**, 032505 (2005).

[16] W. Ubachs, J. C. J. Koelemeij, K. S. E. Eikema, and E. J. Salumbides, *J. Mol. Spectrosc.* **320**, 1 (2016).

[17] E. J. Salumbides, J. C. J. Koelemeij, J. Komasa, K. Pachucki, K. S. E. Eikema, and W. Ubachs, *Phys. Rev. D* **87**, 112008 (2013).

[18] W. Heitler and F. London, *Z. Physik* **44**, 455 (1927).

[19] E. Majorana, *Nuovo Cimento* **8**, 22 (1931).

[20] L. Pauling, *J. Chem. Phys.* **1**, 56 (1933).

[21] S. Weinbaum, *J. Chem. Phys.* **3**, 547 (1935).

[22] B. L. Moiseiwitsch, *Proc. Phys. Soc. A* **69**, 653 (1956).

[23] P. Csavinsky, *J. Chem. Phys.* **31**, 178 (1959).

[24] P. N. Reagan, J. C. Browne, and F. A. Matsen, *Phys. Rev.* **132**, 304 (1963).

[25] B. Liu, *Phys. Rev. Lett.* **27**, 1251 (1971).

[26] J. G. Maas, N. P. F. B. Van Asselt, P. J. C. M. Nowak, J. Los, S. D. Peyerimhoff, and R. J. Buenker, *Chem. Phys.* **17**, 217 (1976).

[27] A. Khan and K. D. Jordan, *Chem. Phys. Lett.* **128**, 368 (1986).

[28] C. W. Bauschlicher, H. Partridge, and D. Ceperley, *Chem. Phys. Lett.* **160**, 183 (1989).

[29] W. Cencek and J. Rychlewski, *J. Chem. Phys.* **102**, 2533 (1995).

[30] W. Cencek and J. Rychlewski, *Chem. Phys. Lett.* **320**, 549 (2000).

[31] J. Xie, B. Poirier, and G. I. Gellene, *J. Chem. Phys.* **122**, 184310 (2005).

[32] W.-C. Tung, M. Pavanello, and L. Adamowicz, *J. Chem. Phys.* **136**, 104309 (2012).

[33] N. Yu and W. H. Wing, *Phys. Rev. Lett.* **59**, 2055 (1987).

[34] A. Carrington, C. H. Pyne, and P. J. Knowles, *J. Chem. Phys.* **102**, 5979 (1995).

[35] M. Stanke, S. Bubin, and L. Adamowicz, *Phys. Rev. A* **79**, 060501 (2009).

[36] D. Sprecher, C. Jungen, W. Ubachs, and F. Merkt, *Faraday Discuss.* **150**, 51 (2011).

[37] D. Sprecher, J. Liu, T. Krähenmann, M. Schäfer, and F. Merkt, *J. Chem. Phys.* **140**, 064304 (2014).

[38] P. Jansen, L. Semeria, L. E. Hofer, S. Scheidegger, J. A. Agner, H. Schmutz, and F. Merkt, *Phys. Rev. Lett.* **115**, 133202 (2015).

[39] C. Jungen, in *Handbook of High-Resolution Spectroscopy, "Elements of Quantum Defect Theory"*, Vol. 1 (John Wiley & Sons, 2011).

[40] P. Jansen, L. Semeria, and F. Merkt, *J. Mol. Spectrosc.* **322**, 9 (2016).

[41] U. Hollenstein, H. Palm, and F. Merkt, *Rev. Sci. Instrum.* **71**, 4023 (2000).

[42] M. Raunhardt, M. Schäfer, N. Vanhaecke, and F. Merkt, *J. Chem. Phys.* **128**, 164310 (2008).

[43] M. Motsch, P. Jansen, J. A. Agner, H. Schmutz, and F. Merkt, *Phys. Rev. A* **89**, 043420 (2014).

- [44] N. Vanhaecke, U. Meier, M. Andrist, B. H. Meier, and F. Merkt, *Phys. Rev. A* **75**, 031402 (2007).
- [45] A. W. Wiederkehr, M. Motsch, S. D. Hogan, M. Andrist, H. Schmutz, B. Lambillotte, J. A. Agner, and F. Merkt, *J. Chem. Phys.* **135**, 214202 (2011).
- [46] A. Osterwalder and F. Merkt, *Phys. Rev. Lett.* **82**, 1831 (1999).
- [47] G. Herzberg, *Annu. Rev. Phys. Chem.* **38**, 27 (1987).
- [48] M. L. Ginter, *J. Chem. Phys.* **42**, 561 (1965).
- [49] W. Lichten, M. V. McCusker, and T. L. Vierima, *J. Chem. Phys.* **61**, 2200 (1974).
- [50] W. Lichten and T. Wik, *J. Chem. Phys.* **69**, 98 (1978).
- [51] M. Kristensen and N. Bjerre, *J. Chem. Phys.* **93**, 983 (1990).
- [52] I. Hazell, A. Norregaard, and N. Bjerre, *J. Mol. Spectrosc.* **172**, 135 (1995).
- [53] C. Focsa, P. F. Bernath, and R. Colin, *J. Mol. Spectrosc.* **191**, 209 (1998).
- [54] M. Schäfer, M. Raunhardt, and F. Merkt, *Phys. Rev. A* **81**, 032514 (2010).
- [55] B. Sanguinetti, H. O. Majeed, M. L. Jones, and B. T. H. Varcoe, *J. Phys. B: At. Mol. Opt. Phys.* **42**, 165004 (2009).
- [56] J. Deiglmayr, H. Herburger, H. Saßmannshausen, P. Jansen, H. Schmutz, and F. Merkt, *Phys. Rev. A* **93**, 013424 (2016).